Journal of Power Sources 375 (2018) 93–101

Contents lists available at ScienceDirect

Journal of Power Sources

journal homepage: www.elsevier.com/locate/jpowsour

Toward practical all-solid-state lithium-ion batteries with high energy density and safety: Comparative study for electrodes fabricated by dry- and slurry-mixing processes

Young Jin Nam, Dae Yang Oh, Sung Hoo Jung, Yoon Seok Jung*

School of Energy and Chemical Engineering, Department of Energy Engineering, Ulsan National Institute of Science and Technology (UNIST), 50 UNIST-gil, Ulsan 44919, Republic of Korea

HIGHLIGHTS

- Slurry-mixed electrodes using polymeric binders suffer from poor ionic contacts.
- Premixing of active materials and SEs significantly increases the capacity.
- Pouch-type ASLBs with high energy density (184 W h kg_{cell}^{-1}) are fabricated.
- Excellent safety for pouch-type ASLBs is demonstrated by cutting and heating tests.

GRAPHICAL ABSTRACT

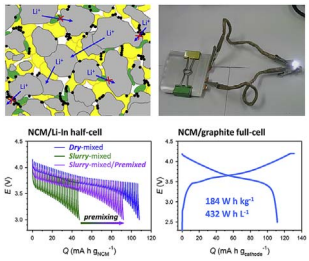

ARTICLE INFO

Keywords:
Batteries
Solid electrolytes
Electrodes
Solid-state batteries
Composites

ABSTRACT

Owing to their potential for greater safety, higher energy density, and scalable fabrication, bulk-type all-solid-state lithium-ion batteries (ASLBs) employing deformable sulfide superionic conductors are considered highly promising for applications in battery electric vehicles. While fabrication of sheet-type electrodes is imperative from the practical point of view, reports on relevant research are scarce. This might be attributable to issues that complicate the slurry-based fabrication process and/or issues with ionic contacts and percolation. In this work, we systematically investigate the electrochemical performance of conventional dry-mixed electrodes and wet-slurry fabricated electrodes for ASLBs, by varying the different fractions of solid electrolytes and the mass loading. This information calls for a need to develop well-designed electrodes with better ionic contacts and to improve the ionic conductivity of solid electrolytes. As a scalable proof-of-concept to achieve better ionic contacts, a premixing process for active materials and solid electrolytes is demonstrated to significantly improve electrochemical performance. Pouch-type 80 × 60 mm^2 all-solid-state $LiNi_{0.6}Co_{0.2}Mn_{0.2}O_2$/graphite full-cells fabricated by the slurry process show high cell-based energy density (184 W h kg^{-1} and 432 W h L^{-1}). For the first time, their excellent safety is also demonstrated by simple tests (cutting with scissors and heating at 110 °C).

1. Introduction

Since the first commercialization of rechargeable lithium-ion batteries (LIBs) in the early 1990s, their use has been widespread for applications involving portable electronic devices [1,2]. Furthermore, extensive progress in LIB technologies in recent years has accelerated the transition from gasoline-engine-powered vehicles to battery electric vehicles (BEVs). This transition is expected to enable reduction of air pollution, enhancement of energy efficiency, and lower dependency on limited fossil fuels [1,2]. Compared with the applications for portable

* Corresponding author.
E-mail address: ysjung@unist.ac.kr (Y.S. Jung).

https://doi.org/10.1016/j.jpowsour.2017.11.031
Received 7 September 2017; Received in revised form 2 November 2017; Accepted 8 November 2017
Available online 23 November 2017
0378-7753/

electronic devices, batteries for BEVs must satisfy much more challenging requirements such as high energy density, long cycle life, safety, and wide ranges of operating temperature [1,3,4]. One of the most critical hurdles in the use of LIBs has been safety. Several recent accidents involved fire or explosions of LIBs in smart phones and BEVs, caused by flammable liquid electrolytes (LEs) [5–10]. Such events have made customers aware of the importance of battery safety. In this regard, all-solid-state lithium-ion batteries (ASLBs), which employ nonflammable solidified electrolytes, are considered a promising alternative to conventional LIBs [6,11–15].

In particular, it is the bulk-type ASLBs based on composite-structured electrodes and electrolyte layers that have the most advantages for BEV applications [6,11,13,16–18]. Bulk-type ASLBs are similar to the already-commercialized LIBs in that both are based on composite-structured electrodes. This implies that high energy density could be achieved by fabricating thick electrodes via a scalable wet-slurry process. In selecting appropriate solid electrolyte (SE) materials for bulk-type ASLBs, high ionic conductivity would be the most important criterion. Conventional LEs exhibit a Li-ion conductivity of $\sim 1 \times 10^{-2}$ S cm^{-1} at room temperature but have a low transference number (0.2–0.4) [6,19]. Because a SE is a single-ion conductor, a SE with an ionic conductivity one order of magnitude lower (1×10^{-3} S cm^{-1}) than that of LEs may result in electrochemical performance comparable to that of conventional LIBs [20]. Furthermore, an ionic conductivity two orders of magnitude lower (1×10^{-4} S cm^{-1}) than that of LEs would be a minimum requirement for SEs in bulk-type ASLBs that could operate at room temperature at moderately low C-rates (e.g., 0.1C) [16,21,22]. Various SEs showing ionic conductivity higher than 1×10^{-4} S cm^{-1} include oxides (e.g., $Li_7La_3Zr_2O_{12}$) [23,24], sulfides (e.g., $Li_{10}GeP_2S_{12}$) [11,17,25], and hydrides, (e.g., $Li_2(BH_4)(NH_2)$) [26]. Although oxide SEs are attractive in terms of processability under ambient conditions with good electrochemical stability, it is extremely challenging to form favorable two dimensional (2D) contacts with active materials because of their brittleness [27]. Thus, a sintering process at elevated temperature is inevitable to wet oxide SEs on active materials [6,27,28]; however, this causes undesirable side reactions, resulting in extremely poor electrochemical performance. To date, the performance of bulk-type ASLBs employing oxide SEs has been reported at elevated temperatures or at room temperature and at extremely low C-rates [28–30]. Alternatively, hybrid bulk-type all-solid-state Li- or Na-ion batteries based on oxide SEs were fabricated by addition of dry or gel polymer electrolytes and/or LE additives [12,31–34].

In contrast, deformability of sulfide SE materials allows the formation of 2D contacts with active materials using a simple pressing process at room temperature, without the use of Li-ion conducting organic additives [6,16,27]. Moreover, extremely high ionic conductivities ($\sim 10^{-2}$ S cm^{-1}) were achieved for several state-of-the-art sulfide materials (e.g., $Li_{10}GeP_2S_{12}$ [11], $Li_7P_3S_{11}$ [25], and $Li_{9.54}Si_{1.74}P_{1.44}S_{11.7}Cl_{0.3}$ [17]). Because of their afore-mentioned critical merits, sulfide SEs are considered to be the most appropriate candidates for making practical bulk-type ASLBs. However, as sulfide SE materials react with water in atmospheric air, generating harmful H_2S gases [6,16,35], manufacturing process in a dry room would be required. Or development of phosphorus-free materials, which is stable in atmosphere, would be imperative for practical applications [16,22,35–37]. Also, the problem of limited electrochemical stability for sulfide SE materials should be addressed by interfacial engineering [38–44].

In most previous reports, composite electrodes for bulk-type ASLBs using sulfide SEs were fabricated by mixing particulate active materials, SEs, and carbon additives in dry condition, followed by cold-pressing [6,11,16,17]. However, the resulting pelletized electrodes were too mechanically unstable to be scaled up [21,43]. Thus, addition of small amounts of polymeric binders is necessary to provide mechanical flexibility and good adhesion between particles and current collectors. In turn, a scalable wet-slurry process using solvent to dissolve polymeric binders should be employed, which allows fabrication of large sheet-type electrodes. The available solvents are restricted to nonpolar or less polar ones such as xylene and toluene, due to severe reactivity of sulfide materials with common polar solvents [21,45]. Moreover, the more complicated homogenization of three components in the polymer-binder-dissolved wet-slurry for ASLB electrodes (active materials, SEs, and carbon additives) is contrasted by the need for only two components for LIB electrodes (active materials and carbon additives) [21]. Overall, the fabrication of sheet-type electrodes for ASLBs by the slurry method is much more complicated than that for well-optimized LIB electrodes. There are only a few reports regarding sheet-type electrodes for ASLBs to date [21,43,46–49], which led our group to investigate fabrication of bulk-type ASLBs using sulfide SEs from a practical point of view.

Herein, we make a comparative investigation of the electrochemical performance of conventional dry-mixed electrodes without polymeric binders, and sheet-type electrodes fabricated using a wet-slurry process with polymeric binders, in various combinations of electrode composition and mass loading. A controlled premixing process for active materials and SEs is introduced as a scalable method to enhance utilization of the active materials in all-solid-state cells. Finally, high cell-based energy density (184 W h kg^{-1} and 432 W h L^{-1}), and excellent safety for 80 × 60 mm^2 pouch-type $LiNi_{0.6}Co_{0.2}Mn_{0.2}$ (NCM622)/graphite all-solid-state full-cells are highlighted.

2. Experimental

2.1. Preparation of materials

Argyrodite Li_6PS_5Cl SE powders were prepared by mechanical-milling and subsequent heat-treatment under inert atmosphere. After a stoichiometric mixture of Li_2S (99.9%, Alfa Aesar), P_2S_5 (99%, Sigma Aldrich), and LiCl (99.99%, Sigma Aldrich) was ball-milled at 600 rpm for 10 h at room temperature in a ZrO_2 vial with ZrO_2 balls using a planetary ball mill (Pulverisette 7 PL; Fritsch GmbH). The resulting powders were heat-treated at 550 °C for 5 h in a sealed quartz tube. The premixing process was carried out by milling a mixture of NCM622 and SE powders with ZrO_2 balls at 1000 rpm for 6 min using Thinky Mixer. $LiNbO_3$ (1.4 wt%) was coated on NCM622 powder using the wet-chemical method, before using the electrodes [16]. The uniform $LiNbO_3$ coating was confirmed by the field-emission scanning electron microscopy (FESEM) image and the corresponding energy dispersive X-ray spectroscopy (EDXS) elemental maps (Fig. S1).

Materials Characterization: The FESEM images were obtained using an S-4800 (Hitachi). Cross-sectional surfaces of the electrodes were prepared by polishing at 5 kV for 13 h with an Ar ion beam (JEOL, SM-0910). The FESEM images and the corresponding EDXS elemental maps of cross-sectioned electrodes were obtained using a JSM-7000F (JEOL). For the XRD measurements, samples were sealed with a beryllium window and mounted on a D8-Bruker Advance diffractometer (Cu K_α radiation: 1.54056 Å) at 40 mA and 40 kV.

2.2. Electrochemical characterization

The Li-ion conductivity of the Li_6PS_5Cl SE pelletized under 370 MPa was measured using an AC (alternating current) impedance method with a Ti/SE/Ti Li-ion blocking cell. The dry-mixed electrodes were obtained by manual mixing of active materials (NCM622), SE powders (Li_6PS_5Cl), and carbon additives (Super C65) with the target compositions. The wet-slurry fabricated electrodes were obtained by the following procedure. Slurries were prepared by mixing targeted amounts of SE powders, active materials (NCM622 or graphite powders), nitrile-butadiene rubber (NBR), and carbon additives (only for cathode) in anhydrous xylene. The Raman and Fourier-transform infrared (FTIR) spectra for NBR are provided in Fig. S2, where the characteristic peaks match well with the functional groups for NBR. After the as-prepared

slurries were coated on current collectors using the doctor blade method, the electrodes were obtained by heating at 120 °C and subsequent drying under vacuum overnight. For fabrication of the NCM622/Li-In half-cells, the mixed electrode powders for dry-mixed electrodes (or the slurry mixed electrodes) were put on the surfaces of the pre-pelletized SE layer (150 mg). For fabrication of the NCM622/graphite full-cells, the SE layers were coated directly on the as-formed graphite electrode by the doctor-blade method using a xylene-NBR-based slurry. The negative electrodes of $Li_{0.5}In$ (nominal composition) powders for the half-cells [12] or the slurry-mixed graphite electrodes for the full-cells were put on the other side of the SE layer. Then, all the assembled components were pressed at 370 MPa in a PEEK (polyether ether ketone) mold (diameter of 13 mm) with Ti metal rods as current collectors. The pelletized NCM622/graphite full-cells were cycled at 0.025C and 30 °C between 2.50 and 4.20 V for the first two cycles, 2.50–4.25 V for the subsequent two cycles, and 2.50–4.30 V for the following cycles. The pouch-type NCM622/graphite full-cells were fabricated by sealing an assembly of the wet-slurry fabricated electrodes and SE layer (positive electrodes: 80 × 60 mm^2, negative electrodes and SE layers: 83 × 63 mm^2) in a pouch, and pressing subsequently at 492 MPa. The pouch-type full-cells were cycled at 0.025C and 25 °C between 2.5 and 4.2 V. All the procedures for fabrication of the electrodes and cells were performed in an Ar-filled dry box in which H_2O was controlled to < 1 ppm. The EIS measurements were performed with amplitude of 10 mV and frequency range from 5 mHz to 1.5 MHz using an Iviumstat (IVIUM Technologies Corp.). After the cells were discharged to 3.7 V (vs. Li/Li^+) at 0.1C at the second cycle, a constant voltage of 3.7 V (vs. Li/Li^+) was applied until the current decreased to 0.025C, followed by rest for 3 h to restore equilibrium. The galvanostatic intermittent titration technique (GITT) measurements were carried out with a pulse current of 0.6C for 60 s and rest for 2 h at the second cycle. The contact areas between NCM622 and SE particles (S) were obtained by the GITT measurements using the following equation [16,21,22].

$$D = \frac{4}{\pi\tau}\left(\frac{m_{NCM}\cdot V_M}{M_{NCM}\cdot S}\right)^2\cdot\left(\frac{\Delta E_S}{\Delta E_t}\right)^2 \quad (1)$$

where D: chemical diffusion coefficient of NCM622, S: contact area between electrolyte and active materials, τ: pulse duration (60 s), ΔE_s: steady-state voltage change, ΔE_t:transient voltage change, M_{NCM}: molecular weight of the host, $Ni_{0.6}Co_{0.2}Mn_{0.2}O_2$ (90.13 g mol^{-1}), m_{NCM}: mass of the host in the sample (varied depending on the mass loading), V_m: molar volume of the sample (the value used was for $LiNi_{1/3}Co_{1/3}Mn_{1/3}O_2$, 20.29 cm^3 mol^{-1}) [50].

The chemical diffusion coefficient (D) of 1.72 × 10^{-11} cm^2 s^{-1} for NCM622 was obtained from a GITT result using a NCM622/Li cell with LE. The surface coverage values were obtained by dividing the contact area between active materials and SEs obtained by the as-described GITT analysis by the surface areas of NCM622 powders obtained by N_2 adsorption-desorption isotherm experiment (0.64 m^2 g^{-1}).

3. Results and discussion

3.1. Comparison of electrodes fabricated by dry-mixing and wet-slurry processes

Two types of composite electrodes for all-solid-state cells were fabricated: i) by dry-mixing active materials with SEs and super C65 in an agate mortar without polymeric binders (Fig. 1a), and ii) by wet-mixing a slurry comprising active materials, SEs, super C65, and NBR in anhydrous xylene (Fig. 1b). The as-prepared slurry was coated on current-collectors of Al or Ni foils for positive and negative electrodes, respectively, followed by drying under vacuum at 120 °C. The resulting sheet-type electrodes exhibited good adhesion to the current collectors (Fig. 1c). Hereafter, the electrodes fabricated by dry-mixing and wet-slurry process are referred to as “dry-mixed” and “slurry-mixed” electrodes, respectively. An argyrodite Li_6PS_5Cl with a Li-ionic conductivity of 3.2 × 10^{-3} S cm^{-1} (after exposure to anhydrous xylene, 2.8 × 10^{-3} S cm^{-1}) at 30 °C (Fig. S3), synthesized by solid-state reaction at 550 °C, was used for the electrodes [51]. Microstructures of the dry- and slurry-mixed electrodes are illustrated in Fig. 1d and e, respectively. For both dry- and slurry-mixed electrodes, SEs make 2D contacts with active materials, providing ionic conduction pathways, while super C65 electronically connects the active materials. However, for slurry-mixed electrodes (Fig. 1e), the added polymeric binders would impede ionic conduction by blocking favorable contacts between active materials and SEs.

Fig. 2 shows the first-cycle charge/discharge voltage profiles for NCM622/Li-In half-cells at 0.1C (0.17 mA g_{NCM622}^{-1}) and at 30 °C, varied by weight fraction of SEs and mass loading. The dry- and slurry-mixed electrodes with a given weight fraction of NCM622 (x) with a lower mass loading are referred to as “DxL” and “WxL”, respectively. Detailed specifications for the electrodes are provided in Table 1. The first-cycle discharge capacity values are summarized in Fig. S4 and Table 1. Three features should be pointed out in the trends of variation in discharge capacity. First, decreasing the weight fraction of active materials caused increased capacity. For example, the discharge capacity of 130 mA h g^{-1} for the D85L electrode was increased to 152 and 155 mA h g^{-1} for the D80L and D70L electrodes, respectively. The higher fraction of active materials (or the lower fraction of SEs) would lead to poorer contacts between active materials and SEs [16,21,22,37,38], and longer percolation pathways of Li^+ ions in the SE regions [38,39]. Both of these imply poor kinetics, which results in low utilization of active materials and poor rate capability. The increased capacities with the higher weight fraction of SEs should be offset by an increased amount of inactive components. In terms of capacity based on the total weight of the electrodes, 80 wt% of active materials showed the highest capacity (Table 1). Second, the electrodes with higher mass loading (28 mg cm^{-2}) showed lower capacity than those with lower mass loading (20 mg cm^{-2}), which is most critical in the case of the lowest weight fraction of SEs (e.g., 130 mA h g^{-1} for D85L vs. 85 mA h g^{-1} for D85H). In conventional LIB electrodes soaked in LEs, the ionic transport in pores (LE regions) acts as the rate determining step when the electrodes become thicker [52]. In this context, the lower capacities of the ASLB electrodes with higher mass loading (or thicker electrodes) could be attributed mostly to Li^+ ion conduction through the SE regions [38,52]. This strongly emphasizes the critical need for SEs with high ionic conductivity. Third and most importantly, the slurry-mixed electrodes significantly underperformed the dry-mixed electrodes. Except for the electrodes of D85H and W85H, which exhibited poor capacities, the gap between the discharge capacities of dry- and slurry-mixed electrodes was 18–35 mA h g^{-1}. The degradation of SE during the wet-slurry process is unlikely because the decrease in conductivity of SE under exposure to anhydrous xylene appeared marginal (Fig. S3b). The presence of insulating polymeric binders that partially block contacts between active materials and SEs (illustrated in Fig. 1e), could be responsible for the poorer performances of the slurry-mixed electrodes than the dry-mixed electrodes [21]. In the cross-sectional FESEM images of the dry-mixed (D85) and slurry-mixed (W85) electrodes and their corresponding elemental maps of Ni, sulfur, and nitrogen (Fig. S5), the regions for Ni match with that for nitrogen. This observation would indicate that the surface of NCM622 be covered with the NBR binders, which agrees with the illustration of disruption in ionic pathways by binders in Fig. 1e. The rate capabilities of dry- and slurry-mixed electrodes, varied by the weight fraction of active materials and mass loadings, are also shown in Fig. 3 and Fig. S6. The trends of rate capabilities are well in line with the results of discharge capacities (Fig. 2 and Fig. S4). It is also noted that the gap between the rate capability of the lower and higher mass-loaded electrodes became larger at higher C-rates.

In an attempt to understand the variations in discharge capacities

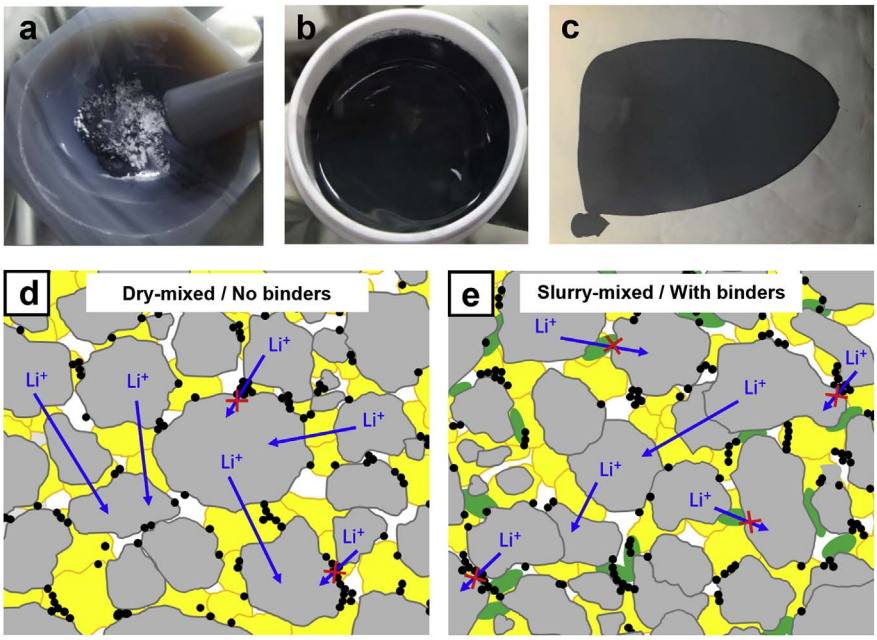

Fig. 1. Comparison of a-solid-state lithium-ion battery (ASLB) electrodes fabricated by dry-mixing and wet-slurry processes. Photographs of a) a dry-mixture of active materials, SEs, and super C65 without polymeric binders and b) a slurry comprised of active materials, SEs, super C65, and polymeric binders in xylene. c) Sheet-type NCM622 electrode fabricated by the wet-slurry process. Schematic diagrams representing the microstructures of ASLB electrodes a) by dry-mixing process without binders and b) by wet-slurry process using binders. Active materials, SEs, super P, and polymeric binders (NBR) are shown in gray, yellow, black, and green, respectively. (For interpretation of the references to colour in this figure legend, the reader is referred to the web version of this article.)

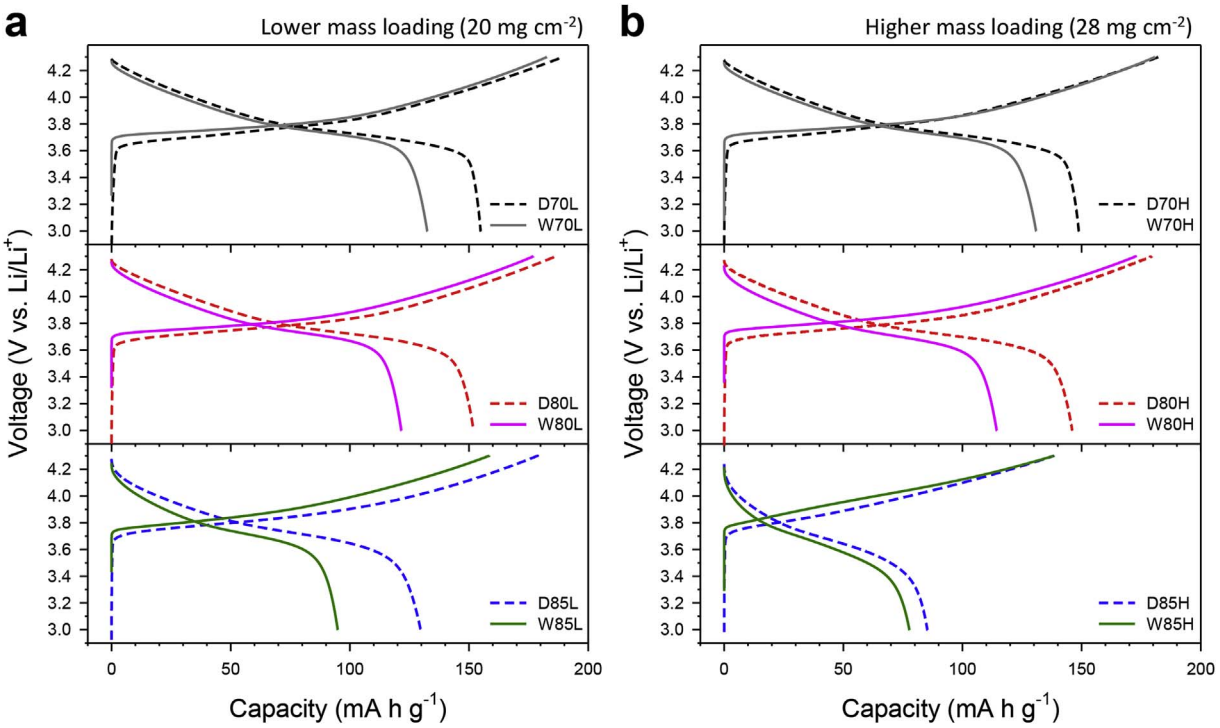

Fig. 2. First-cycle charge-discharge voltage profiles at 0.1C and 30 °C for all-solid-state NCM622/Li-In half-cells employing dry- and slurry-mixed electrodes with a) the lower mass loading and b) the higher mass loading of NCM622.

and rate performances observed, complementary analysis was carried out using FESEM, electrochemical impedance spectroscopy (EIS), and GITT measurements. FESEM images of top views of the dry- and slurry-mixed electrodes and their corresponding EDXS elemental maps for sulfur are shown in Fig. 4. The elemental maps show more segregated SEs for the electrodes with higher weight fraction of active materials (D85 and W85) and for the slurry-mixed electrodes (W70 and W85), than for the dry-mixed electrodes (D70 and D85). The more segregated SEs indicate poorer ionic percolation, which could explain the capacity of the slurry-mixed electrodes being lower than that of the dry-mixed electrodes and of the electrodes with lower weight fractions of SEs (Fig. 2, S4, 3, S6).

Nyquist plots of the dry-mixed and slurry-mixed electrodes in Fig. 5 show one depressed semicircle followed by Warburg tail. The numbers were normalized in Ω g because the resistance is inversely proportional to the surface area of active materials, and thus the mass loading. The intercept values at the x-axis indicate the resistance assigned to the SE layer [16,38]. The semicircles at high- and mid-frequency range are interpreted as contributions by charge transfer resistance at electrode-SE interfaces and/or electronic contributions of the composite electrodes [16,38,53]. The Warburg tail at low frequency stems from Li-ion diffusion in active materials [16,38]. The EIS spectra were fitted using an equivalent circuit (Fig. S7a), and the R2 values, which could result from multiple contributions such as charge transfer resistance and

Table 1
Characteristics of dry- and slurry-mixed NCM622 electrodes for ASLBs.

Process	Sample name	Composition[a]	$Q_{0.1C}$[b]		R [Ω g]	Surface coverage of SEs onto active materials [%]
			[mA h g_{NCM}^{-1}]	[mA h $g_{electrode}^{-1}$]		
Dry-mixing	D70L	69.1/29.6/1.3/0	155	107	0.18	25.2
	D70H		149	103	0.23	
	D80L	79.2/19.5/1.3/0	152	120	0.19	15.4
	D80H		146	116	0.28	
	D85L	84.3/14.4/1.3/0	130	109	0.26	12.9
	D85H		85	72	0.41	
Wet-slurry	W70L	68.1/29.2/1.3/1.4	133	90	0.29	17.5
	W70H		131	89	0.50	
	W80L	78.1/19.2/1.3/1.4	122	95	0.81	14.0
	W80H		114	89	1.22	
	W85L	83.1/14.2/1.3/1.4	95	79	0.92	5.8
	W85H		78	65	1.37	
	Premixed W85L		127	106	0.44	9.4

[a] Weight ratio of active material to SE to Super P to NBR.
[b] The first-cycle discharge capacity at 0.1C.

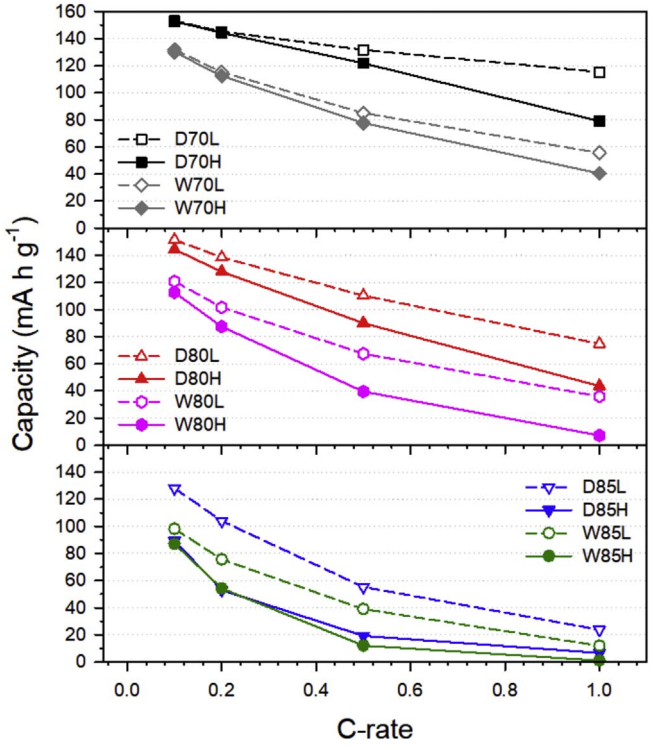

Fig. 3. Discharge capacities for all-solid-state NCM622/Li-In half-cells cycled between 3.0 and 4.3 V (vs. Li/Li^+) varied by C-rates at 30 °C. The C-rates for charge and discharge were the same.

electronic resistance, are plotted in Fig. S7b. In line with the results of discharge capacities and rate performances, the resistance was increased by increasing the weight fraction of active materials, by increasing the mass loading, and by adding polymeric binders (for the slurry-mixed electrodes). In particular, it should be noted that the resistance value extracted from the amplitude of the semicircle in the Nyquist plot is an extensive property dependent on the interfacial contact area. Thus, the higher resistance of slurry-mixed electrodes than for dry-mixed electrodes could be explained by unfavorable wetting of SEs onto active materials due to the presence of insulating NBR binders.

The transient discharge voltage profiles from GITT experiments are presented in Fig. 6. The corresponding polarization data obtained by subtracting closed-circuit voltage (CCV) from quasi-open-circuit voltage (QOCV) are also plotted, and perfectly agree with the discharge capacities (Fig. 2), the rate performances (Fig. 3), and the EIS spectra (Fig. 5). Importantly, interfacial surface coverage of SEs onto active materials were deduced by analysis using GITT [16,21,22]. The dry-mixed electrodes with the highest weight fraction of SEs (D70L or D70H) exhibited the highest surface coverage (25.2%). The low value indicates incompleteness of solid-solid contacts between active materials and SEs. This also might be attributed to micro-voids in the inner regions of NCM622 particles, which could not be accessed by the SEs outside [54,55] and/or to inaccurate factors used for the governing equation (see Experimental for the details). The electrodes with lower weight fraction of SEs showed much lower surface coverage values than did the electrodes with higher weight fraction of SEs (Table 1). Importantly, the surface coverage values turned out to be far less for the slurry-mixed electrodes than for the dry-mixed electrodes (Table 1). For instance, the surface coverage of 25.2% for the D70 electrode was decreased to 17.5% by adding NBR (for the W70 electrode). This result corroborates that the insulting polymeric binders interrupt direct ionic contacts between SEs and active materials; thereby degrading the electrochemical performance, as illustrated in Fig. 1e.

3.2. Electrodes fabricated by premixing process

From the systematic and complementary analysis results in the previous section, it is evident that solid-solid ionic contacts between active materials and SEs become poorer when lower amount of SEs are used and/or when polymeric binders are included in the ASLB composite electrodes, which is necessary for practical ASLB with high energy density. In this regard, premixing of active materials (NCM622) and SEs by ball-milling in a dry condition prior to wet-slurry fabrication was attempted to ensure favorable ionic contacts without hindrance by polymeric binders, as illustrated in Fig. 7a. After premixing, the characteristic XRD peaks for NCM622 and argyrodite Li_6PS_5Cl remained intact, indicating negligible chemical interaction between active materials and SEs (Fig. 7b).

The slurry-mixed electrode with the lowest amount of SE (W85L) was chosen to examine the effect of premixing on electrochemical performances. FESEM images of cross-sectioned views of the W85L electrode fabricated with and without premixing, and their

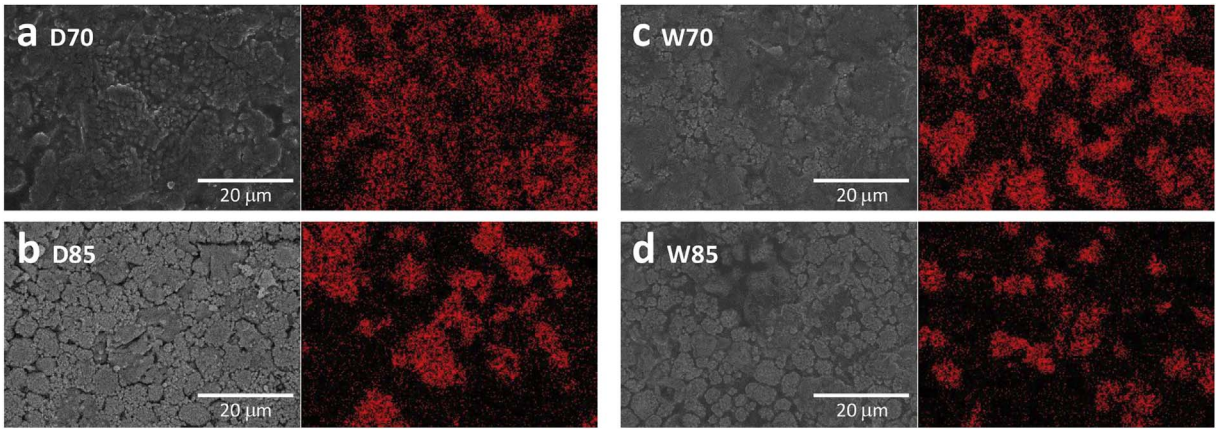

Fig. 4. FESEM surface images of NCM622 electrodes fabricated by dry-mixing process with a) ~70 wt% (D70) and b) ~85 wt% of NCM622 (D85) and wet-slurry process using NBR with c) ~70 wt% (W70) and d) ~85 wt% (W85) of NCM622. Their corresponding EDXS elemental maps for sulfur are also shown.

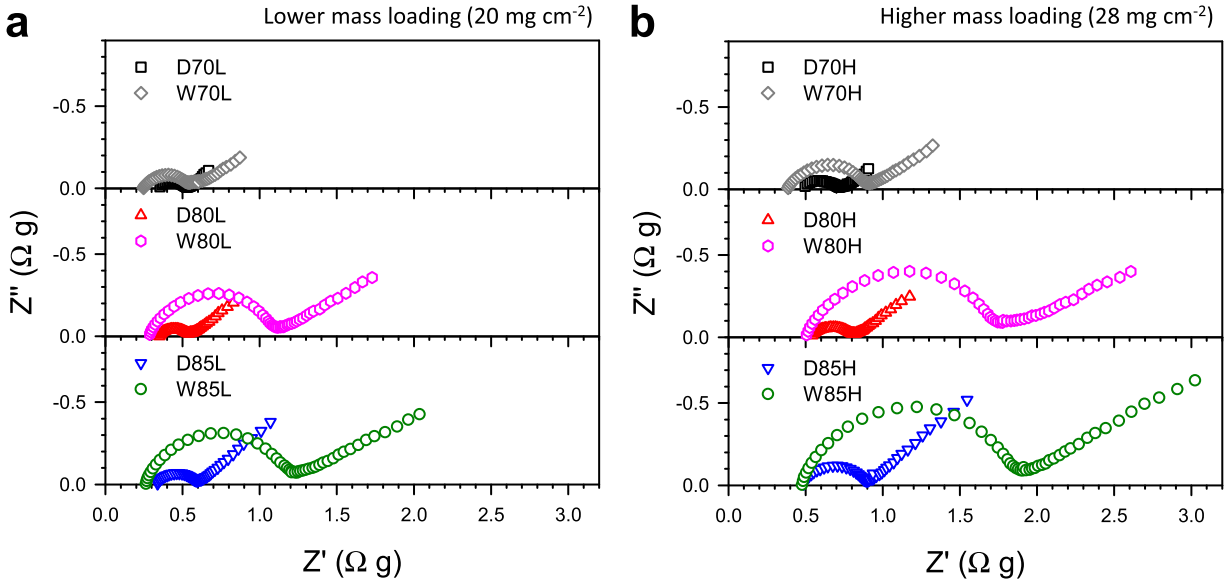

Fig. 5. Nyquist plots at 30 °C for all-solid-state NCM622/Li-In half-cells employing dry-and slurry-mixed electrodes with a) the lower mass loading and b) the higher mass loading.

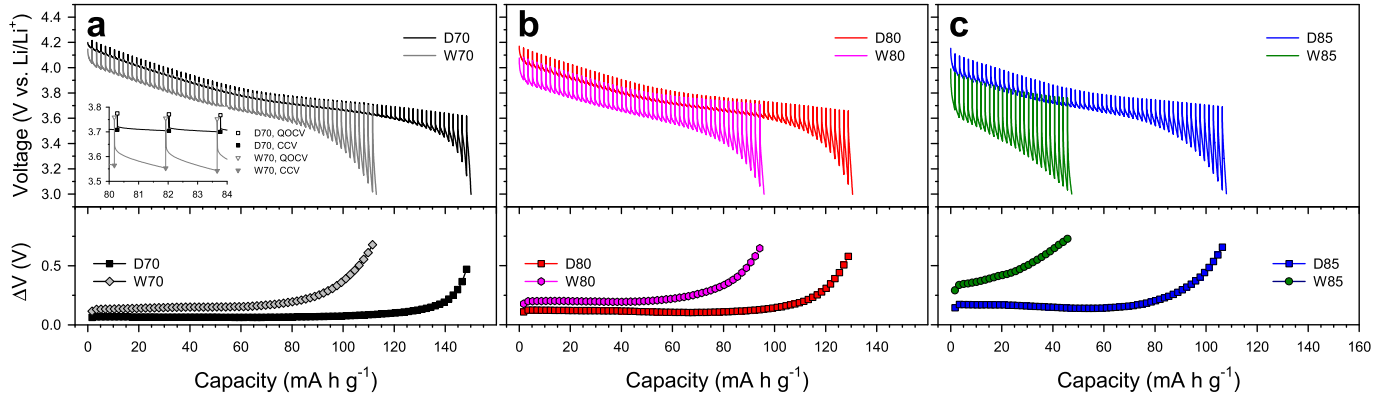

Fig. 6. Transient discharge voltage profiles at 30 °C and their corresponding polarization (ΔV) curves for all-solid-state NCM622/Li-In half-cells employing dry- and slurry-mixed electrodes with a) ~70 wt%, b) ~80 wt%, and c) ~85 wt% NCM622, obtained by GITT. The enlarged view where QOCV and CCV are indicated is shown in the inset in a. The polarization data were plotted by subtracting CCV from QOCV in the transient voltage profiles in transient discharge voltage profiles.

corresponding EDXS elemental maps for sulfur (green) and Ni (red) are compared in Fig. 7c. The signals of sulfur are more homogeneous and overlapped more with the regions for Ni signals for a premixed electrode than for a conventional one, implying closer contacts between active materials and SEs in the former.

The electrochemical performance of the W85L electrodes with and without premixing, are compared in Fig. 7d–f. The first-cycle discharge capacity was significantly increased by premixing: from 92 to 129 mA h g^{-1}. This improvement of the electrochemical performance by premixing is in line with the decreased amplitude of the semicircle

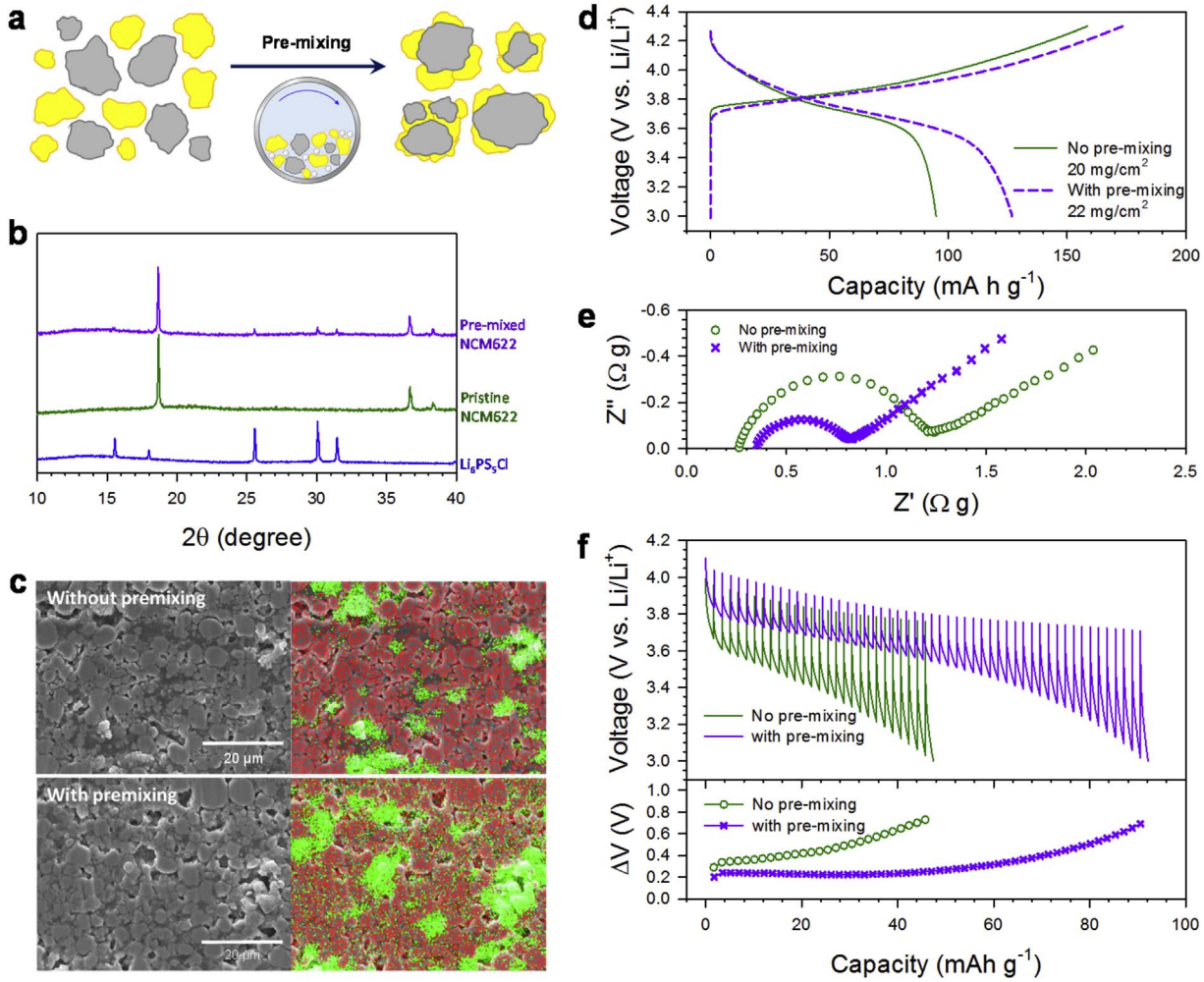

Fig. 7. Results of NCM622 electrodes fabricated by wet-slurry process using a premixed powder of NCM622 and SEs. a) Schematic diagram of premixing process for NCM622 and SE powders by mechanical milling. b) XRD patterns of Li_6PS_5Cl, pristine NCM622, and NCM622 premixed with Li_6PS_5Cl. c) Cross-sectional FESEM images of wet-mixed NCM622 electrodes without and with premixing process and their corresponding EDXS elemental maps for Ni (red) and sulfur (green). d) First-cycle charge-discharge voltage profiles at 0.1C, e) Nyquist plots, and f) transient discharge voltage profiles and their corresponding polarization (ΔV) curves for slurry-mixed NCM622 electrodes without and with premixing process, and their corresponding polarization curves. (For interpretation of the references to colour in this figure legend, the reader is referred to the web version of this article.)

by approximately half in the Nyquist plot (Fig. 7e, Table 1) and the significantly decreased polarization for the premixed electrodes in the GITT result (Fig. 7f). Importantly, the dramatic increase of surface coverage of SEs onto NCM622 by premixing (from 5.8% to 9.4%) was also confirmed. These results emphasize the beneficial effect of premixing on utilization of active materials in terms of favorable ionic contacts. Unfortunately, at higher C-rates of 0.5C or 1C, the improvement from premixing appeared marginal (Fig. S8). It is speculated that the ionic conductivity of SEs must be considerably more improved to achieve better high-rate performance. Damage to SEs by mechanical impacts during the premixing process also cannot be ruled out to explain the unsatisfactory high-rate capability of a premixed electrode. Further optimization of the premixing process will be our next mission.

3.3. All-solid-state NCM622/Graphite full-cells

NCM622/graphite ASLBs were fabricated using the slurry-mixed electrodes. For the full-cell, the slurry-mixed graphite electrode showing the first-cycle discharge capacity of 330 mA h g^{-1} at 0.025C and 30 °C was used (Fig. S9). SE layers were coated on the graphite electrodes by wet-slurry process before combining with the NCM622 electrodes. Two types of full-cells were fabricated: a conventional pelletized cell and an 80 × 60 mm^2 pouch-type cell (Fig. 8a). The detailed specifications for the NCM622/graphite full-cells are presented in Table 2. Fig. 8b shows their first-cycle charge-discharge profiles for the pelletized and pouch-type NCM622/graphite full-cells at 0.025C at 25 °C and 30 °C, respectively. The first-cycle discharge capacities for the pelletized and pouch-type NCM622/graphite full-cells were 121 and 112 mA h $g_{NCM622\ electrode}{}^{-1}$, respectively, which translates into 190 and 184 W h kg^{-1} based on total weight of the electrodes (active materials, SEs, carbon additives, polymeric binders, and current collectors). In turn, the volumetric energy density of the pouch-type full-cell is calculated to be 432 W h L^{-1}. The NCM622/graphite full-cell also showed a stable cycling performance at 0.025C (the inset in Fig. 8b).

The safety performance of the pouch-type NCM622/graphite full-cell was assessed by simple tests. First, a pouch-cell that was fully charged to 4.3 V at 0.025C was cut with scissors. As shown in Fig. 8c and Movie S1, the cut pouch-cell remained working and illuminated a white light emitting diode (LED) without any noticeable events indicating a need for safety concerns. This result indicates that the SE layers are mechanically robust, and able to avoid short-circuits between positive and negative electrodes after cutting. It also shows that they are thermally stable against the Joule-heat generated by the instant short current while being cut [5,56,57]. In the second test, a fully charged pouch-cell was subjected to heating at 111 °C on a hot plate for > 1 h. It also remained intact and illuminated the white LED (Fig. 8d and Movie S2). This is in contrast to swelling and irreversible

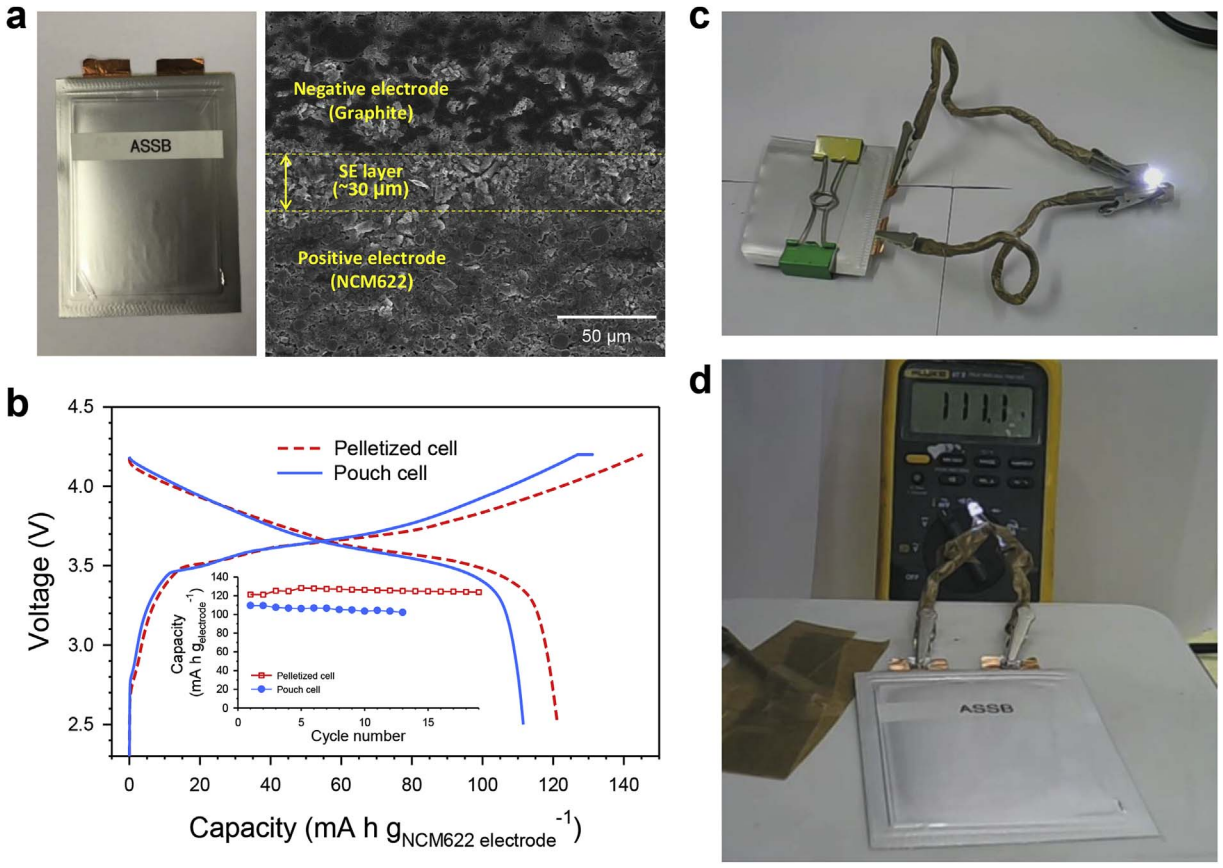

Fig. 8. Results of NCM622/graphite all-solid-state full-cells. a) Photograph of 80 × 60 mm^2 pouch-type NCM622/graphite full-cell and its cross-sectional FESEM image. b) First-cycle charge-discharge voltage profiles of pelletized and pouch-type full-cells of NCM622/graphite at 0.025C. The pelletized cell and pouch-cell were tested at 30 °C and 25 °C, respectively. The detailed specifications are provided in Table 2. Photographs of 80 × 60 mm^2 pouch-type NCM622/graphite all-solid-state full-cells c) after cutting with scissors and d) being placed on the hot plate at 111 °C for > 1 h.

damage for the conventional LIBs based on LEs [56–58]. The temperature of 111 °C for the experiment was set based on the limited thermal stability of the pouch materials. Even higher temperature than 111 °C might not cause serious effects on the electrochemical and safety performance of the ASLB [17,21]. Although more sophisticated and elaborate experiments are required to make a fairer evaluation of safety performance in terms of quantitative analysis, to our knowledge, our results are the first demonstration of the excellent safety of pouch- and bulk-type ASLBs based on sulfide SEs.

Supplementary video related to this article can be found at http://dx.doi.org/10.1016/j.jpowsour.2017.11.031.

4. Conclusions

In summary, the electrochemical performances of dry- and slurry-mixed NCM622 electrodes, varied by different fractions of SEs and mass loading, were systematically investigated. The presence of polymeric binders (NBR) for the slurry-mixed electrodes and the lower fractions of

Table 2
Characteristics of NCM622/graphite all-solid-state full-cells.

Cell type		Composition[a]	Mass loading [mg cm^{-2}]	Thickness [μm]	Energy density[b]
Pelletized cell	Positive electrode	79.2/19.5/1.3/0	37	155	190 W h kg^{-1}[c]
	SE layer	0/98.5/0/1.5	7.5	45	202 W h kg^{-1}[d]
	Negative electrode	58.6/39.1/0/2.3	27	138	
Pouch-cell (80 × 60 mm^2)	Positive electrode	68.1/29.2/1.3/1.4	21	88	184 W h kg^{-1}
	SE layer	0/98.5/0/1.5	4.9	30	432 W h L^{-1}
	Negative electrode	58.6/39.1/0/2.3	13	65	(405 mA h)
Pouch-cell (88 × 53 mm^2) in previous work[e]	Positive electrode	59/34/5/2	35	250	89 W h kg^{-1}[f]
	SE layer	0/98/0/2	32.6[f]	200	139 W h L^{-1}[f]
	Negative electrode	95/0/0/5	14	100	(125 mA h)

[a] Weight ratio of active material to SE to Super P to NBR.
[b] Based on total weights of the electrodes, SE layers, and current collectors.
[c] For upper cut-off voltage of 4.2 V.
[d] For upper cut-off voltage of 4.3 V.
[e] From previous result [48].
[f] Estimated values based on the data in the previous result [48].

SEs resulted in lower capacity and poorer rate capability, which was attributed to poorer ionic contacts between active materials and SEs. This was evidenced by complementary analysis using EIS, GITT, and FESEM. Higher mass loading also degraded the electrochemical performance significantly, implying that the bottleneck in overall kinetics for the thicker electrodes relates to Li-ion transport in the SE regions. These results call for a need to design composite electrodes for better ionic contacts and percolation, and to develop highly conductive SEs. A scalable process for premixing active materials and SEs prior to preparation of the slurry, as the proof-of-concept for achieving more intimate contacts, was demonstrated to significantly improve electrochemical performance. Finally, the high energy density (184 W h kg^{-1} and 432 W h L^{-1}) and excellent safety of the 80 × 60 mm^2 pouch-type NCM622/graphite full-cells, were successfully demonstrated.

Acknowledgements

This research was supported by Hyundai Motor Group, by the Technology Development Program to Solve Climate Changes of the National Research Foundation of Korea (NRF) funded by the Ministry of Science & ITC (grant no. 2017M1A2A2044501), and by the Materials and Components Technology Development Program of MOTIE/KEIT (10077709).

Appendix A. Supplementary data

Supplementary data related to this article can be found at http://dx.doi.org/10.1016/j.jpowsour.2017.11.031.

References

[1] J.B. Goodenough, Y. Kim, Chem. Mater 22 (2010) 587–603.
[2] J.-M. Tarascon, Phil. Trans. R. Soc. A 368 (2010) 3227–3241.
[3] A. Manthiram, X. Yu, S. Wang, Nat. Rev. Mater 2 (2017) 16103.
[4] V. Etacheri, R. Marom, R. Elazari, G. Salitra, D. Aurbach, Energy Environ. Sci. 4 (2011) 3243–3262.
[5] R. Spotnitz, J. Franklin, J. Power Sources 113 (2003) 81–100.
[6] Y.S. Jung, D.Y. Oh, Y.J. Nam, K.H. Park, Isr. J. Chem. 55 (2015) 472–485.
[7] T. Inoue, K. Mukai, ACS Appl. Mat. Inter 9 (2017) 1507–1515.
[8] S. Liberatore, Samsung's Battery Woes Continue as Lawsuits Spread to Galaxy Note 5, S6 and S7 Models, (2017) http://www.dailymail.co.uk/sciencetech/article-4542628/Samsung-hit-lawsuits-claiming-devices-exploded.html (accessed 17.05.25).
[9] V. Woollaston, New Blow for Tesla: Fire in the 'world's Safest Electric Car' Began in Vehicle's Battery, (2013) http://www.dailymail.co.uk/sciencetech/article-2442392/New-blow-Tesla-Fire-worlds-safest-electric-car-began-vehicles-battery.html (accessed 13.10.03).
[10] J. Kalhoff, G.G. Eshetu, D. Bresser, S. Passerini, ChemSusChem 8 (2015) 2154–2175.
[11] N. Kamaya, K. Homma, Y. Yamakawa, M. Hirayama, R. Kanno, M. Yonemura, T. Kamiyama, Y. Kato, S. Hama, K. Kawamoto, A. Mitsui, Nat. Mater 10 (2011) 682–686.
[12] X. Han, Y. Gong, K.K. Fu, X. He, G.T. Hitz, J. Dai, A. Pearse, B. Liu, H. Wang, G. Rubloff, Y. Mo, V. Thangadurai, E.D. Wachsman, L. Hu, Nat. Mater 16 (2017) 572–579.
[13] J. Janek, W.G. Zeier, Nat. Energy 1 (2016) 16141.
[14] Y. Wang, W.D. Richards, S.P. Ong, L.J. Miara, J.C. Kim, Y. Mo, G. Ceder, Nat. Mater 14 (2015) 1026–1032.
[15] K. Kerman, A. Luntz, V. Viswanathan, Y.-M. Chiang, Z. Chen, J. Electrochem. Soc. 164 (2017) A1731–A1744.
[16] K.H. Park, D.Y. Oh, Y.E. Choi, Y.J. Nam, L. Han, J.-Y. Kim, H. Xin, F. Lin, S.M. Oh, Y.S. Jung, Adv. Mater 28 (2016) 1874–1883.
[17] Y. Kato, S. Hori, T. Saito, K. Suzuki, M. Hirayama, A. Mitsui, M. Yonemura, H. Iba, R. Kanno, Nat. Energy 1 (2016) 16030.
[18] Z. Lin, Z. Liu, W. Fu, N.J. Dudney, C. Liang, Angew. Chem. Int. Ed. 52 (2013) 7460–7463.
[19] K. Xu, Chem. Rev. 104 (2004) 4303–4417.
[20] M. Doyle, T.F. Fuller, J. Newman, Electrochim. Acta 39 (1994) 2073–2081.
[21] D.H. Kim, D.Y. Oh, K.H. Park, Y.E. Choi, Y.J. Nam, H.A. Lee, S.-M. Lee, Y.S. Jung, Nano Lett. 17 (2017) 3013–3020.
[22] Y.E. Choi, K.H. Park, D.H. Kim, D.Y. Oh, H.R. Kwak, Y.-G. Lee, Y.S. Jung, ChemSusChem 10 (2017) 2605–2611.
[23] Y.Y. Ren, K. Chen, R.J. Chen, T. Liu, Y.B. Zhang, C.W. Nan, J. Am. Ceram. Soc. 98 (2015) 3603–3623.
[24] H. El-Shinawi, G.W. Paterson, D.A. MacLaren, E.J. Cussen, S.A. Corr, J. Mat. Chem. A 5 (2017) 319–329.
[25] Y. Seino, T. Ota, K. Takada, A. Hayashi, M. Tatsumisago, Energy Environ. Sci. 7 (2014) 627–631.
[26] A. Unemoto, M. Matsuo, S. Orimo, Adv. Funct. Mater 24 (2014) 2267–2279.
[27] A. Sakuda, A. Hayashi, M. Tatsumisago, Sci. Rep. 3 (2013) 2261.
[28] S. Ohta, J. Seki, Y. Yagi, Y. Kihira, T. Tani, T. Asoka, J. Power Sources 265 (2014) 40–44.
[29] A. Aboulaich, R. Bouchet, G. Delaizir, V. Seznec, L. Tortet, M. Morcrette, P. Rozier, J.-M. Tarascon, V. Viallet, Adv. Energy Mater 1 (2011) 179–183.
[30] S. Ohta, S. Komagata, J. Seki, T. Saeki, S. Morishita, T. Asaoka, J. Power Sources 238 (2013) 53–56.
[31] H. Gao, L. Xue, S. Xin, K. Park, J.B. Goodenough, Angew. Chem. Int. Ed. 56 (2017) 5541–5545.
[32] Z.Z. Zhang, Q.H. Zhang, J.A. Shi, Y.S. Chu, X.Q. Yu, K.Q. Xu, M.Y. Ge, H.F. Yan, W.J. Li, L. Gu, Y.S. Hu, H. Li, X.Q. Yang, L.Q. Chen, X.J. Huang, Adv. Energy Mater 7 (2017) 1601196.
[33] H.W. Kim, P. Manikandan, Y.J. Lim, J.H. Kim, S.C. Nam, Y. Kim, J. Mat. Chem. A 4 (2016) 17025–17032.
[34] Y. Li, W. Zhou, X. Chen, X. Lu, Z. Cui, S. Xin, L. Xue, Q. Jia, J.B. Goodenough, P. Natl. Acad. Sci. U. S. A 113 (2016) 13313–13317.
[35] H. Muramatsu, A. Hayashi, T. Ohtomo, S. Hama, M. Tatsumisago, Solid State Ionics 182 (2011) 116–118.
[36] G. Sahu, Z. Lin, J. Li, Z. Liu, N. Dudney, C. Liang, Energy Environ. Sci. 7 (2014) 1053.
[37] A. Banerjee, K.H. Park, J.W. Heo, Y.J. Nam, C.K. Moon, S.M. Oh, S.-T. Hong, Y.S. Jung, Angew. Chem. Int. Ed. 55 (2016) 9634–9638.
[38] B.R. Shin, Y.J. Nam, D.Y. Oh, D.H. Kim, J.W. Kim, Y.S. Jung, Electrochim. Acta 146 (2014) 395–402.
[39] W. Zhang, D.A. Weber, H. Weigand, T. Arlt, I. Manke, D. Schro¨der, R. Koerver, T. Leichtweiss, P. Hartmann, W.G. Zeier, J. Janek, ACS Appl. Mat. Inter 9 (2017) 17835–17845.
[40] Y.S. Tian, T. Shi, W.D. Richards, J.C. Li, J.C. Kim, S.H. Bo, G. Ceder, Energy Environ. Sci. 10 (2017) 1150–1166.
[41] Y. Zhu, X. He, Y. Mo, ACS Appl. Mat. Inter 7 (2015) 23685–23693.
[42] F. Han, Y. Zhu, X. He, Y. Mo, C. Wang, Adv. Energy Mater 6 (2016) 1501590.
[43] Y.J. Nam, S.J. Jo, D.Y. Oh, J.M. Im, S.Y. Kim, J.H. Song, Y.-G. Lee, S.-Y. Lee, Y.S. Jung, Nano Lett. 15 (2015) 3317–3323.
[44] N. Ohta, K. Takada, L. Zhang, R. Ma, M. Osada, T. Sasaki, Adv. Energy Mater 18 (2006) 2226–2229.
[45] D.Y. Oh, Y.J. Nam, K.H. Park, S.H. Jung, S.-J. Cho, Y.K. Kim, Y.-G. Lee, S.-Y. Lee, Y.S. Jung, Adv. Energy Mater 5 (2015) 1500865.
[46] T. Inada, K. Takada, A. Kajiyama, M. Kouguchi, H. Sasaki, S. Kondo, M. Watanabe, M. Murayama, R. Kanno, Solid State Ionics 158 (2003) 275–280.
[47] T. Inada, T. Kobayashi, N. Sonoyama, A. Yamada, S. Kondo, M. Nagao, R. Kanno, J. Power Sources 194 (2009) 1085–1088.
[48] S. Ito, S. Fujiki, T. Yamada, Y. Aihara, Y. Park, T.Y. Kim, S.-W. Baek, J.-M. Lee, S. Doo, N. Machida, J. Power Sources 248 (2014) 943–950.
[49] D.Y. Oh, D.H. Kim, S.H. Jung, J.-G. Han, N.-S. Choi, Y.S. Jung, J. Mat. Chem. A 5 (2017) 20771–20779.
[50] K.M. Shaju, G.V.S. Rao, B.V.R. Chowdari, J. Electrochem. Soc. 151 (2004) A1324–A1332.
[51] H.-J. Deiseroth, S.-T. Kong, H. Eckert, J. Vannahme, C. Reiner, T. Zaiss, M. Schlosser, Angew. Chem. Int. Ed. 47 (2008) 755–758.
[52] N. Ogihara, Y. Itou, T. Sasaki, Y. Takeuchi, J. Phys. Chem. C 119 (2015) 4612–4619.
[53] M. Gaberscek, J. Moskon, B. Erjavec, R. Dominko, J. Jamnik, Electrochem. Solid-State Lett. 11 (2008) A170–A174.
[54] R. Koerver, I. Aygün, T. Leichtweiß, C. Dietrich, W. Zhang, J.O. Binder, P. Hartmann, W.G. Zeier, J. Janek, Chem. Mater 29 (2017) 5574–5582.
[55] Y.-K. Sun, Z. Chen, H.-J. Noh, D.-J. Lee, H.-G. Jung, Y. Ren, S. Wang, C.S. Yoon, S.-T. Myung, K. Amine, Nat. Mater 11 (2012) 942–947.
[56] G.-H. Kim, K. Smith, K.-J. Lee, S. Santhanagopalan, A. Pesaran, J. Electrochem. Soc. 158 (2011) A955–A969.
[57] C.F. Lopez, J.A. Jeevarajan, P.P. Mukherjee, J. Electrochem. Soc. 162 (2015) A1905–A1915.
[58] Y.S. Jung, A.S. Cavanagh, L. Gedvilas, N.E. Widjonarko, I.D. Scott, S.-H. Lee, G.-H. Kim, S.M. George, A.C. Dillon, Adv. Energy Mater 2 (2012) 1022–1027.